



## OPEN ACCESS

## EDITED BY

He Li,  
Berkeley Lab (DOE), United States

## REVIEWED BY

Zhongbin Pan,  
Ningbo University, China  
Ravi Kumar Cheedarala,  
Changwon National University,  
Republic of Korea  
Zhiyuan Huang,  
Berkeley Lab (DOE), United States

## \*CORRESPONDENCE

Sivasubramanian Mahadevan,  
✉ m.sivasubramanian@klu.ac.in  
Cristiano Fragassa,  
✉ cristiano.fragassa@unibo.it

RECEIVED 20 June 2023

ACCEPTED 18 July 2023

PUBLISHED 28 July 2023

## CITATION

Armstrong M, Mahadevan S,  
Selvapalam N, Santulli C, Palanisamy S  
and Fragassa C (2023), Augmenting the  
double pipe heat exchanger efficiency  
using varied molar Ag ornamented  
graphene oxide (GO) nanoparticles  
aqueous hybrid nanofluids.  
*Front. Mater.* 10:1240606.  
doi: 10.3389/fmats.2023.1240606

## COPYRIGHT

© 2023 Armstrong, Mahadevan,  
Selvapalam, Santulli, Palanisamy and  
Fragassa. This is an open-access article  
distributed under the terms of the  
[Creative Commons Attribution License  
\(CC BY\)](https://creativecommons.org/licenses/by/4.0/). The use, distribution or  
reproduction in other forums is  
permitted, provided the original author(s)  
and the copyright owner(s) are credited  
and that the original publication in this  
journal is cited, in accordance with  
accepted academic practice. No use,  
distribution or reproduction is permitted  
which does not comply with these terms.

# Augmenting the double pipe heat exchanger efficiency using varied molar Ag ornamented graphene oxide (GO) nanoparticles aqueous hybrid nanofluids

Michael Armstrong<sup>1</sup>, Sivasubramanian Mahadevan<sup>1\*</sup>,  
Narayanan Selvapalam<sup>2</sup>, Carlo Santulli<sup>3</sup>,  
Sivasubramanian Palanisamy<sup>4</sup> and Cristiano Fragassa<sup>5\*</sup>

<sup>1</sup>School of Mechanical, Aero, Auto and Civil Engineering, Kalasalingam Academy of Research and Education, Virudhunagar, Tamil Nadu, India, <sup>2</sup>School of Advanced Sciences, Kalasalingam Academy of Research and Education, Virudhunagar, Tamil Nadu, India, <sup>3</sup>School of Science and Technology (SST), Università Degli Studi di Camerino, Camerino, Italy, <sup>4</sup>Department of Mechanical Engineering, Dilkap Research Institute of Engineering and Management Studies, Karjat, Raigad, India, <sup>5</sup>Department of Industrial Engineering, University of Bologna, Bologna, Italy

The optimization of heat transfer in heat exchanging equipment is paramount for the efficient management of energy resources in both industrial and residential settings. In pursuit of this goal, this empirical study embarked on enhancing the heat transfer performance of a double pipe heat exchanger (DPHX) by introducing silver (Ag)-graphene oxide (GO) hybrid nanofluids into the annulus of the heat exchanger. To achieve this, three distinct molar concentrations of Ag ornamented GO hybrid nanoparticles were synthesized by blending GO nanoparticles with silver nitrate at molarities of 0.03 M, 0.06 M, and 0.09 M. These Ag-GO hybrid nanoparticles were then dispersed in the base fluid, resulting in the formation of three distinct hybrid nanofluids, each with a consistent weight percentage of 0.05 wt%. Thorough characterization and evaluation of thermophysical properties were performed on the resulting hybrid nanomaterials and nanofluids, respectively. Remarkably, the most significant enhancement in heat transfer coefficient, Nusselt number, and thermal performance index (62.9%, 33.55%, and 1.29, respectively) was observed with the 0.09 M Ag-GO hybrid nanofluid, operating at a Reynolds number of 1,451 and a flow rate of 47 g/s. These findings highlight the substantial improvement in thermophysical properties of the base fluid and the intensification of heat transfer in the DPHX with increasing Ag molarity over GO. In summary, this study emphasizes the vital importance of optimizing the molarity of the material, which also plays a significant role in nanoparticle synthesis to achieve the optimal amplification of heat transfer.

## KEYWORDS

Ag-GO aqueous hybrid nanofluids, thermophysical properties, double pipe heat exchanger, convective heat transfer coefficient, nanoparticles, synthesis, characterization

## 1 Introduction

For several decades, researchers have been studying the thermal amplification of double pipe heat exchangers (DPHX), as they have significant scientific implications. DPHX is widely used due to its simple design, high-pressure area, short floor space, ease of cleaning, low cost, and its usage in various applications such as chemical plants, power plants, solar energy systems, air conditioning systems, and waste heat recovery systems (H. Li et al., 2022; Maghrabie et al., 2021; Ghalebaz et al., 2022). Recently, researchers have focused on enhancing the heat transfer properties of conventional base fluids (water, ethylene glycol, oil, etc.), by incorporating nanomaterials with high thermo-physical properties (Cheedarala et al., 2016; Mbambo et al., 2020; Boudraa and Bessaih, 2021). Different types of nanofluids have been developed, including metals, metal oxides, and carbon-based nanofluids, either as mono or hybrid forms (Sharma and Mishra, 2022; K. Kumar et al., 2022; Mousavi et al., 2021). Within the realm of carbon allotropes, graphene (Gr) has captivated significant interest due to its exceptional properties. As a result, it has also garnered considerable attention within the field of thermal investigations (Cheedarala et al., 2015; Yarmand et al., 2015; Yu et al., 2020). For example, Mehrali et al. (2015) examined the Gr nanoplatelet nanofluid in a heat exchanger with varying nanoparticle weight percent (0.025–0.1 wt%) and found a 12%–28% increase in thermal conductivity and a 15% increase in heat transfer coefficient at 0.1 wt%. Yarmand et al. (2015) decorated Gr nanoplatelets with silver (Ag) nanoparticles and observed a 22.2% increase in thermal conductivity, 1.3 times increase in viscosity, and a 32.70% enhancement in Nusselt number (at  $Re = 17,500$ ) with 0.1 wt% in distilled water.

Although graphene nanoparticles possess outstanding properties, their difficulty in large-scale preparation and hydrophobic nature have led to increased interest in their derivative, graphene oxide (GO). GO has gained interest as a heat transfer fluid due to its simplicity of wide-scale synthesis, hydrophilic nature, greater thermal conductivity and surface-to-volume ratio, and superior surface chemistry to support and retain doping species intrinsically (Mehrali et al., 2016; Cheedarala and JungSong, 2019). Several researchers have utilized GO either as a homogeneous or combined it with metal nanoparticles to form hybrid nanofluids with improved thermophysical, optical, and chemical properties than base fluids (Banerjee, 2018; Majumder and Gangopadhyay, 2022). Karabulut et al. (2020) applied GO/distilled water nanofluid in copper pipe with turbulent flow under constant heat flux, reporting a 48% increase in maximum heat transfer coefficient at 0.02 vol% and 1.5 L/min flow rate ( $Re 5,032$ ). Ranjbarzadeh et al. (2022) used GO nanoparticles at 0–0.15 vol% to enhance heat exchanger efficiency, thermal conductivity, and convective heat transfer in industrial cooling systems, achieving a 34.7% increase in convective heat transfer coefficient and 9.64% in friction factor over the base fluid. Kumar et al. (2021) investigated GO and rGO-CuO nanofluid heat transfer performance in a laminar regime in a heat exchanger tube, finding a 53.33% increase in heat transfer coefficient using rGO-CuO nanofluid at 0.05 wt% over DI water. In the different aspects, the researcher Hui et al. (2014) experimented with Ag-GO nanohybrids using different concentrations of silver nitrate ( $AgNO_3$ , 0.1 M, 0.2 M, and 0.6 M) and ultrasonication time to control the size of Ag

nanoparticles. Similarly, Lozano-Steinmetz et al. (2022) explored the impact of different concentrations of Ag (0.01 M, 0.1 M, and 1 M) on the thermophysical properties of reduced graphene oxide (rGO). Their findings revealed that the use of 0.1 M concentration of Ag significantly boosted the nanofluid's properties in comparison to other concentrations, suggesting its application in heat transfer systems. Building upon the foundations laid by these scientific reports and knowledge, this study endeavours to investigate the heat transfer performance in an annulus of the DPHX by utilizing varied lower molar (0.03 M, 0.06 M, and 0.09 M) Ag ornamented GO hybrid nanofluids at 0.05 wt%. The materials characterization, stability, thermo-physical properties, and thermal performance of this novel approach in double pipe heat exchangers have been meticulously explored and analysed. This study unlocks exciting new insights into the thermal enhancement of double pipe heat exchangers utilizing varied molar Ag-GO hybrid nanofluids.

## 2 Materials and procedures

### 2.1 Synthesis of Ag-GO nanoparticles

The production of graphene oxide (GO) nanoparticles was carried out using a modified Hummer's method (Hummers and Offeman, 1958; Hui et al., 2014; Le Ba et al., 2020; Cobos et al., 2020; Gul et al., 2023), utilizing high-quality analytical-grade reagents in its fresh state from renowned manufacturers such as Sigma Aldrich, United States; Otto Chemie Private Ltd.; Avra Synthesis Private Ltd.; and Sisco Research Laboratories Pvt Ltd., India. Figures 1A–C provides a visual depiction showcasing the chemical structural formation, schematic representation, and preparation process of Ag-GO hybrid nanofluids. The Ag-GO nanohybrids were prepared by combining freshly synthesized GO nanoparticles with varied molar concentrated Ag metal precursors. First, GO nanosuspensions were ultrasonicated in double distilled water (DW) for 2 h. Then, appropriate concentrations of  $AgNO_3$  solutions (0.03 M, 0.06 M, and 0.09 M) were blended with Vitamin C (ascorbic acid, 1 mL,  $10^{-3}$  M) as a reducing agent and trisodium citrate (1 mL,  $10^{-3}$  M) as a stabilizing agent. This process yielded a varied Ag-concentrated solution, which was stirred continuously for 1 h at room temperature. The reducing and stabilizing agents played a significant role in controlling the size and morphology of the Ag nanoparticles. Furthermore, the varied Ag ornamented GO nanostructures were obtained by titrating the prepared Ag (0.03 M, 0.06 M, 0.09 M) solutions uniformly with a definite GO solution.

It resulted in a 0.03 M, 0.06 M, and 0.09 M Ag ornamented GO nano solution that was stirred constantly in the magnetic stirrer at 90 rpm without adding light or heating during the 48 h until a fusion of Ag-GO hybrid solution was formed. The solution was then sonicated for 2 h to ensure better dispersions. The Ag-GO solution was filtered, rinsed with DW and alcohol until the potential of hydrogen (pH) was close to 7.4–7.6, and then treated in a vacuum hot air oven at 50°C to yield 0.03 M, 0.06 M, and 0.09 M Ag ornamented GO hybrid nanoparticles.

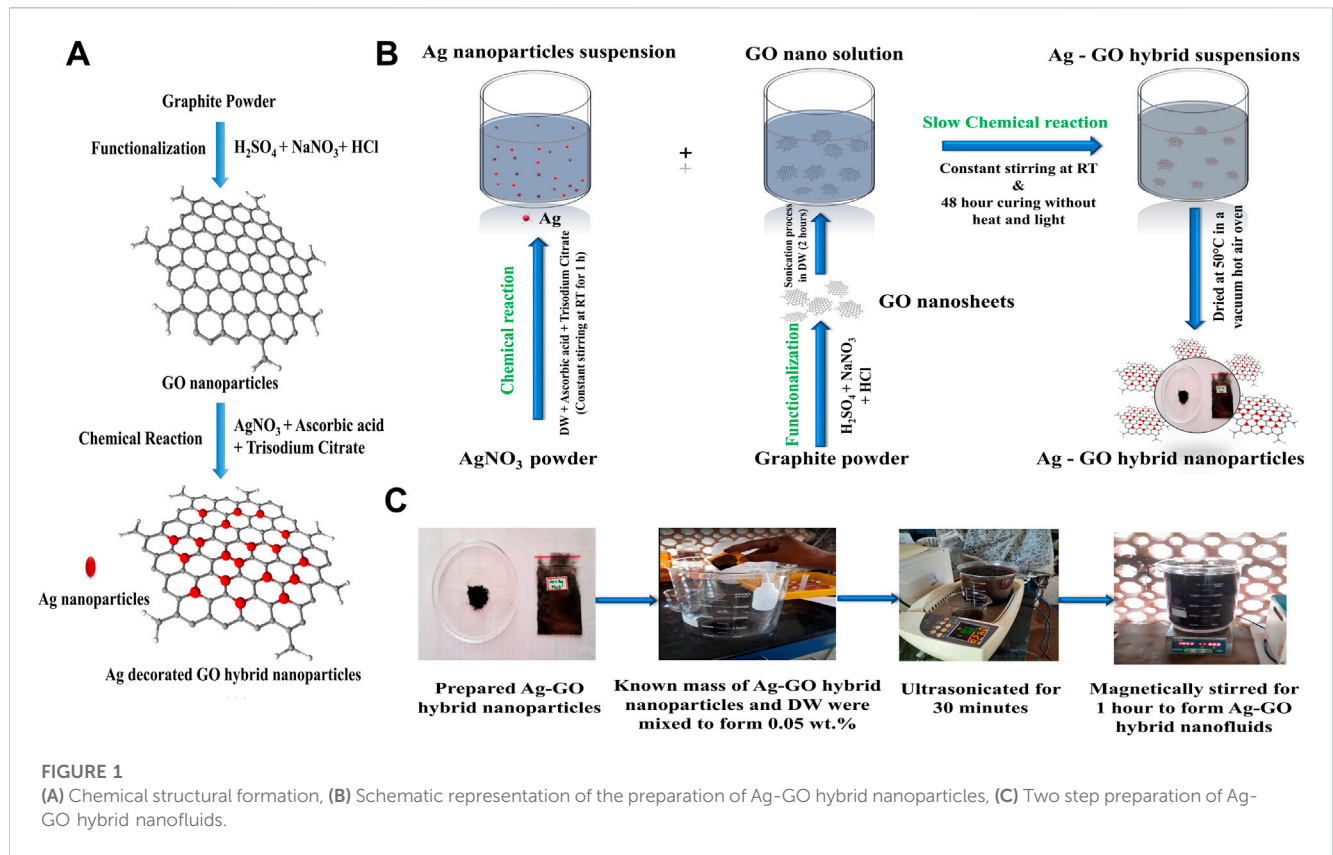


**FIGURE 1** (A) Chemical structural formation, (B) Schematic representation of the preparation of Ag-GO hybrid nanoparticles, (C) Two step preparation of Ag-GO hybrid nanofluids.

## 2.2 Preparation of Ag-GO nanofluids

The preparation of Ag-GO nanofluids is a crucial step in ensuring optimal heat transfer performance. In our study, we prepared Ag-GO nanofluids at different concentrations (0.03 M, 0.06 M, and 0.09 M) using a two-step process from double distilled water (DW). To achieve optimal dispersion, each synthesized Ag-GO nanohybrids was mixed with a known mass ( $m_{bf}$ ) of DW, then ultrasonicated for 30 min and stirred for 1 h using a magnetic stirrer. To ensure uniformity, we maintained a constant weight percentage ( $\phi$ ) of 0.05% by controlling the nanoparticle's mass ( $m_{np}$ ) for all samples using the digital weighing machine of accuracy 0.001 g, as estimated using Eq. 1.

$$m_{np} = \frac{\phi \cdot m_{bf}}{1 - \phi} \tag{1}$$

By carefully controlling the synthesis process, we aimed to achieve maximum stability, dispersion, and optimal thermophysical properties of the Ag-GO nanofluids.

## 2.3 Characterization of Ag-GO nanomaterials

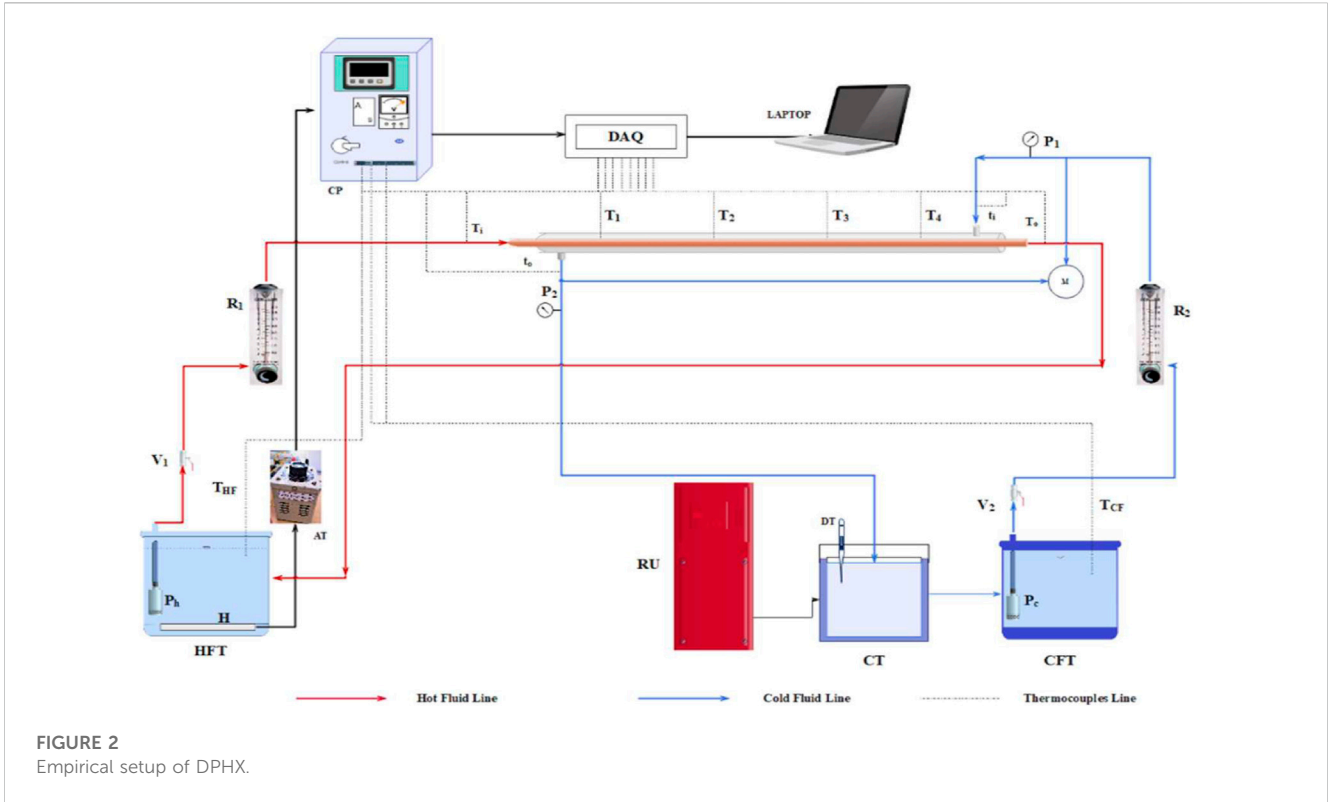
The morphology and composition of the synthesized Ag-GO hybrid nanoparticles were analysed using a range of sophisticated instruments, including Powder X-ray diffraction (XRD-D8 Advance

ECO Bruker) with a copper anode ( $k\lambda = 1.54060$ ) in a  $2\theta$  range of  $10^\circ$ – $80^\circ$ , High Resolution Transmission Electron Microscope (HRTEM, JEM-2100 Plus, JEOL Japan, at 200 KV), Scanning Electron Microscope (SEM, EVO 18, CARL ZEISS, Jena, Germany) at 30 kV, Fourier Transform Infrared Spectrophotometer (IR Tracer-100 Shimadzu), Particle Size Analyzer (Horiba SZ-100Z), Energy Dispersive X-Ray Spectrometer (EDAX, Quantax 200 with X-Flash), UV-visible Spectrometer (SL210, Elico, India).

The thermophysical properties of the nanofluids were evaluated using a KD2 Pro thermal property analyser (Decagon, United States, Accuracy:  $\pm 5\%$ ), which utilized the transient hotwire line method to measure the thermal conductivity with an exposure limit of 0.02–2 W/m K. The viscosity and surface tension were measured using LVDVE (Brookfield Engineering Labs, United States, Accuracy:  $\pm 1\%$ ) and SITA Dynotester (SITA process solution, Germany, Accuracy:  $\pm 0.1\%$ ), respectively.

## 2.4 Experimental design and methodology

Figure 2 showcases the schematic representation of the experimental setup and fluid flow configurations employed to amplify the heat transfer within a double pipe heat exchanger (DPHX). The setup is composed of an inner copper pipe serving as a hot fluid side with an effective length of 0.990 m and inner diameter of 0.022 m. The cold fluid, which is a nanofluid, flows



through a Chlorinated polyvinyl chloride (CPVC) pipe acted as an outer annulus pipe of 1 m length with an inner diameter of 0.034 m. The empirical circuit also includes hot and cold side fluid tanks (HFT, CFT), Valves ( $V_1$ ,  $V_2$ ), submersible pumps ( $P_h$ ,  $P_c$ ), rotameters ( $R_1$ ,  $R_2$ ), pressure gauges ( $P_1$ ,  $P_2$ ), manometer (M), data acquisition system (DAQ, Make: National Instruments), and a heating element with the digital controller (Selec TC533BX). The control panel system (CP) is linked to the autotransformer (AT) (primary voltage: 240 VAC) to regulate the heat flow rate, maintain steady-state temperatures, and control the overall temperature of the system via DAQ. Ten T-type thermocouples and a digital thermometer (DT) were utilized to monitor temperatures at various locations in the empirical system. The double-pipe heat exchanger is well-wrapped with glass wool, aluminium foil and cotton threads to decrease heat loss. The pump is employed to counter-currently drive fluids from the hot and cold fluid tanks into the inner and annulus side of the pipe. The exit fluids from both ends were then directed to the appropriate collecting tanks to create equilibrium conditions for reprocessing. The flow rate of hot and cold fluids was regulated using two rotameters, with flow rates ranging from 8 to 47 g/s for the cold fluid side (35°C) to achieve the laminar flow regime (Reynolds number 250–1,451), and a constant input temperature and flow rate of the hot fluid side was maintained at 55°C and 17 g/s for the entire set of readings. The convective heat transfer coefficient, thermal performance index, effectiveness, and friction factor of different concentrations (0.03 M, 0.06 M, 0.09 M) of Ag-GO hybrid nanofluid with an analogous weight percentage of 0.05 wt% were investigated independently. The observations were acquired from the average of five sets, and the system was held for 30 min to achieve the equilibrium condition for each set of readings.

### 3 Data reduction

#### 3.1 Solving equations

The ensuing equation represents the heat released by the hot fluid side and the heat absorbed by the cold fluid side (Kern, 1950; Thulukkanam, 2013).

$$Q_h = \dot{m}_h c_{ph} (T_i - T_o); Q_c = \dot{m}_c c_{pc} (t_o - t_i) \tag{2}$$

To elucidate the heat transfer mechanism of the Ag-GO hybrid nanofluids, the amount of heat gained by the nanofluids and its overall heat transfer rate are represented by (Karabulut et al., 2020; Kumar et al., 2021)

$$Q_{nf} = \dot{m}_{nf} c_{pnf} (t_o - t_i)_{nf} \tag{3}$$

$$Q_{avg} = \frac{Q_h + Q_{nf}}{2} \tag{4}$$

The empirical heat transfer coefficient, as per Newton’s Law of Cooling, can be mathematically represented by the following equation (Duangthongsuk and Wongwises, 2009; Iyahraja et al., 2019; Subramanian et al., 2020).

$$h_{nf} = \frac{Q_{avg}}{A(T_{wall} - T_{b_{nf}})} \tag{5}$$

Here,  $T_{wall} = \frac{T_1 + T_2 + \dots + T_n}{n}$ , and  $n = 4$ ;  $T_{b_{nf}}$ —bulk fluid temperature (Hussein, 2017)

$$T_{b_{nf}} = \left( \frac{t_i + t_o}{2} \right)_{nf} \tag{6}$$

The nanofluid’s empirical Nusselt number, Reynolds number, and Prandtl number were determined by using (Goodarzi et al., 2016; Iyahraja et al., 2019)

$$Nu_{nf} = \frac{h_{nf} D_h}{k_{nf}} \tag{7}$$

where  $D_h$  is the hydraulic diameter,  $D_h = D_i - d_o$

$$Re_{nf} = \frac{4m_{nf}}{\pi(d_o + D_i)\mu_{nf}} \tag{8}$$

$$Pr_{nf} = \frac{\mu_{nf} c_{nf}}{k_{nf}} \tag{9}$$

The empirical friction factor was determined by measuring the pressure drop of the annulus pipe and applied in the equation (Goodarzi et al., 2016)

$$\Delta P_{nf} = 2f_{nf}(\rho_{nf} V_{nf}^2)(L/D_h)\left(\frac{\mu_b}{\mu_w}\right)^{-0.14} \tag{10}$$

$$\text{Effectiveness, } \epsilon = \frac{1 - e^{(-NTU(1-Z))}}{1 - Z * e^{(-NTU(1-Z))}} \tag{11}$$

Where  $Z = C_{min}/C_{max}$

Number of Transfer Units,

TABLE 1 Uncertainty analysis.

Factors	Uncertainty range
Nu	± 5.610%
Re	± 1.303%
Q	± 4.160%
h	± 5.433%
f	± 4.127%

$$NTU = \frac{Q_{avg}}{C_{min} * (\Delta T)_{LMTD}} \tag{12}$$

Where

$$(\Delta T)_{LMTD} = \frac{((T_i - t_o) - (T_o - t_i))}{\ln((T_i - t_o)/(T_o - t_i))}$$

### 3.2 Validation of experimental data

The experimental friction factor data for DW were validated by employing the Darcy friction factor equation (Eq. 13). (Iyahraja et al., 2019)

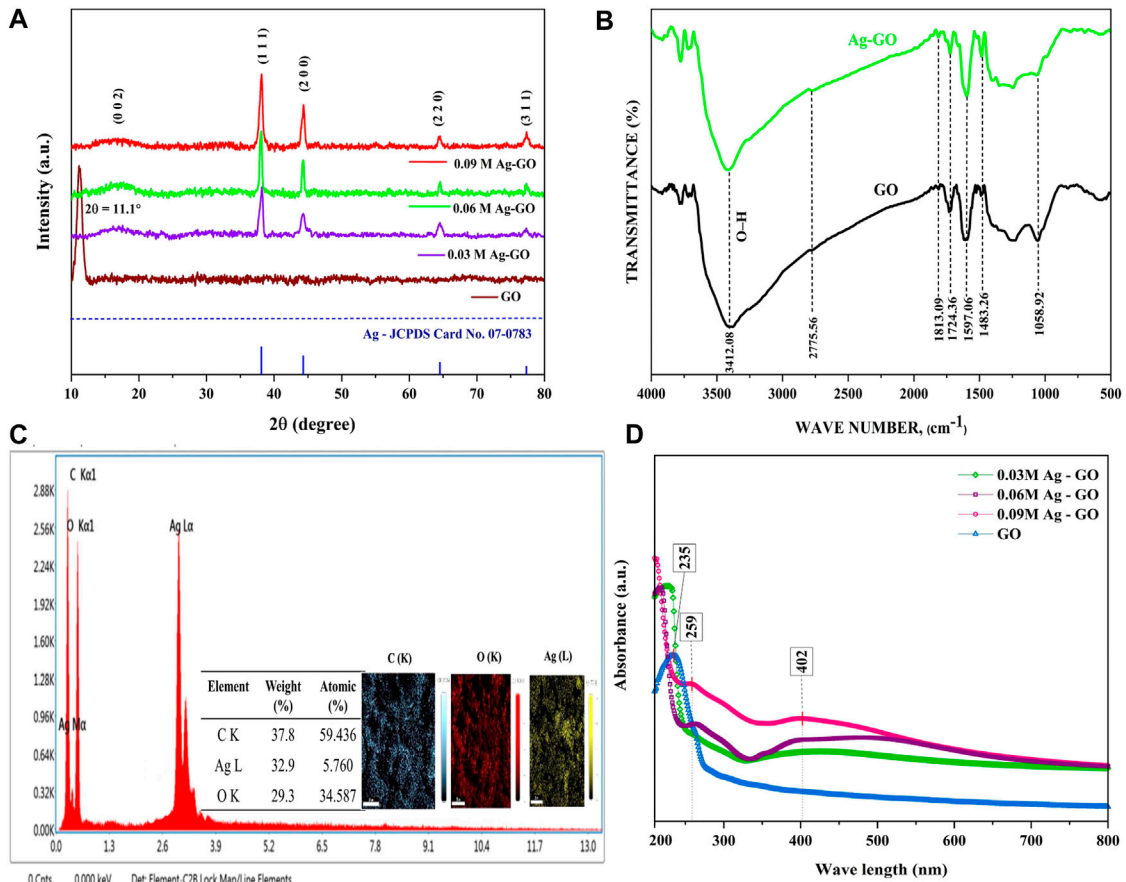
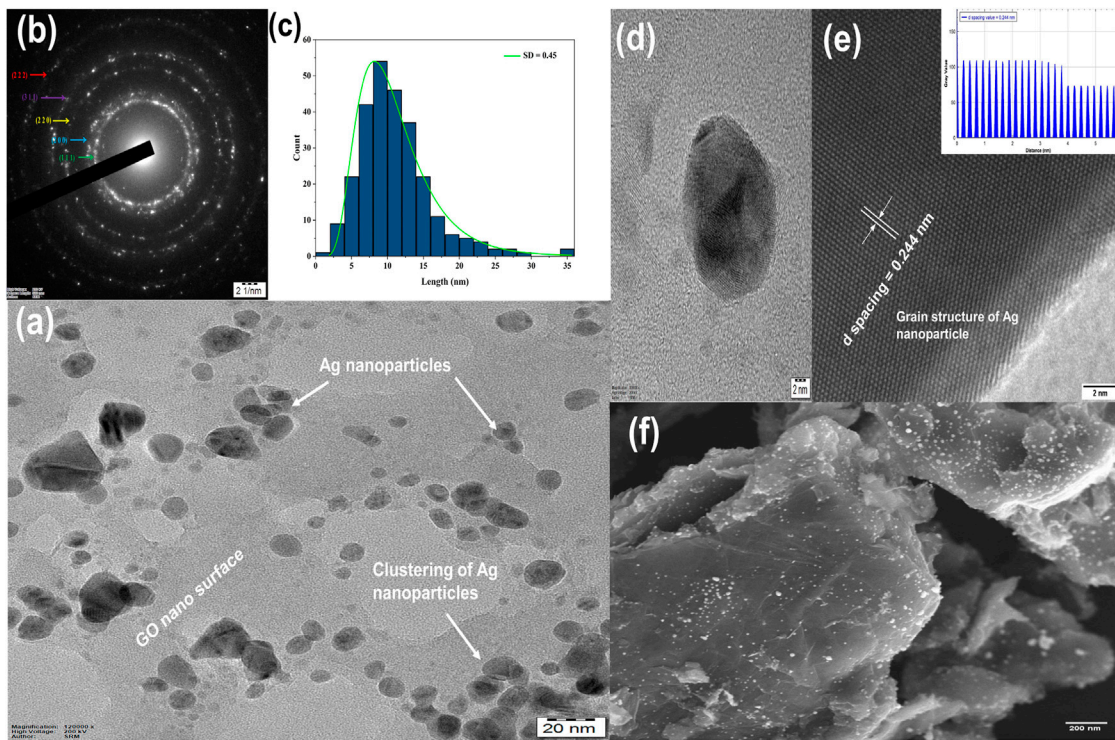


FIGURE 3 (A) XRD, (B) FTIR, (C) EDS, (D) UV Analysis of Ag-GO hybrid nanofluids.



**FIGURE 4** (A) TEM, (B) SAED, (C) Particle Size Distribution, (D,E) HR-TEM, (F) SEM analysis of 0.09 M Ag-GO hybrid nanofluids.

Friction factor,

$$f_o = \frac{64}{Re} \tag{13}$$

In addition, the empirical Nusselt number correlations available in the literatures were used to verify the experimental Nusselt number outcomes for DW. These included the Sieder-Tate equation (Eq. 14) [(Armstrong et al., 2021b; Hussein, 2017), Hausen equation (Eq. 15) (Brebba and Rahman, 2000; Lu and Wang, 2008), Stephan equation (Eq. 16) (Jacimovic, Genic, and Lelea, 2018), B. Jacimovic et al. correlation (Eq. 17) (Jacimovic, Genic, and Lelea, 2018), Leveque equation (Eq. 18) (Bertsche et al., 2015), and Shah equation (Eq. 19) (Hussein, 2017; Jacimovic, Genic, and Lelea, 2018). The Nusselt number correlations were selected based on their previous usage in similar studies and their appropriateness for the present study’s experimental conditions.

$$Nu = 1.86 (Gz)^{1/3} \left( \frac{\mu_b}{\mu_w} \right)^{0.14} \tag{14}$$

$$Nu = \left\{ 3.66 + 1.2 \left( \frac{d_o}{D_i} \right) + \left[ 1 + 0.14 \left( \frac{d_o}{D_i} \right)^{-0.5} \right] \left( \frac{0.19 Gz^{0.8}}{1 + (0.117 Gz^{0.467})} \right) \right\} \left( \frac{Pr_{bmf}}{Pr_w} \right)^{0.11} \tag{15}$$

$$Nu = 3.657 + \left( \frac{0.0677 Gz^{1.33}}{1 + (0.1 Pr^{0.17} Gz^{0.83})} \right) \tag{16}$$

$$Nu = 3.657 + \left( \frac{0.01 Gz^{1.7}}{1 + (0.01 Gz^{1.3})} \right) \left( \frac{\mu_{bmf}}{\mu_w} \right)^{0.14} \tag{17}$$

$$Nu = 1.615 (Gz)^{1/3} \tag{18}$$

$$Nu = \begin{cases} 1.953 (Gz)^{-1/3}, Gz \leq 33.33 \\ 4.364 + 0.0722 (Gz)^{-1}, Gz > 33.33 \end{cases} \tag{19}$$

Where Graetz number,  $Gz = \frac{RePrD_h}{L}$

### 3.3 Uncertainty assessment in experimentation

In any testing and evaluation process, empirical mistakes are inevitable in the real-world context. To assess the reliability of the gathered information, the uncertainty was estimated using Moffat’s technique (Moffat, 1985), which employs partial differential equations to evaluate the recorded findings. Since the findings are influenced by multiple factors, the square root of the sum of the instrumental and measurement errors was used. The uncertainty of instruments such as voltmeter, ammeter, thermocouple, rotameter, and manometer were determined to be ±0.5% of F.S, ±0.51% of F.S, ±0.1°C, ±0.1% and ±4% respectively, with temperature and mass flow rate as the primary sources of measurements.

$$R = R(x_1 + x_2 + x_3 + \dots + x_n)$$

To calculate the uncertainty of the independent factors, the sensitivity coefficient was maintained at just under 5R, and the root sum square technique was employed.

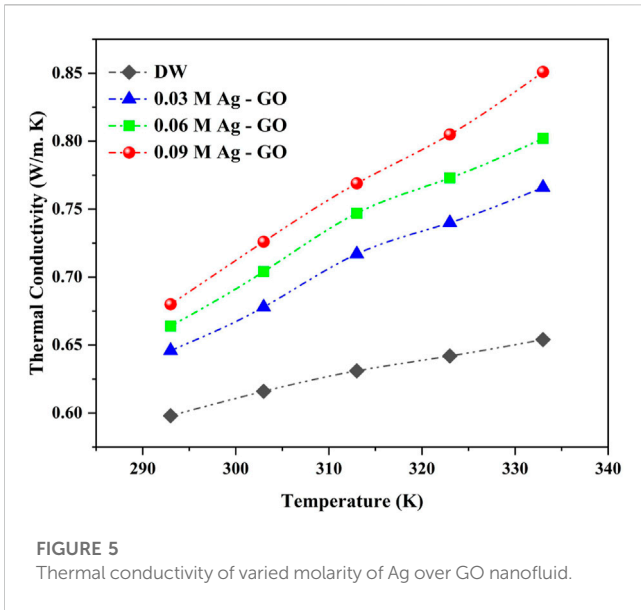


FIGURE 5 Thermal conductivity of varied molarity of Ag over GO nanofluid.

$$\delta R = \left[ \sum_{i=1}^n \left( \frac{\partial R}{\partial x_i} \delta x_i \right)^2 \right]^{1/2}$$

The uncertainties of the heat transfer rate (Q), convective heat transfer coefficient (h), Reynolds number (Re), Nusselt number (Nu) and friction factor (f) were computed using the following equations.

$$\left[ \frac{UQ}{Q} \right] = \left[ \left( \frac{Um}{Q} \frac{\partial Q}{\partial m} \right)^2 + \left( \frac{Ut_o}{Q} \frac{\partial Q}{\partial t_o} \right)^2 + \left( \frac{Ut_i}{Q} \frac{\partial Q}{\partial t_i} \right)^2 \right]^{1/2}$$

$$\left[ \frac{Uh}{h} \right] = \left[ \left( \frac{UQ}{h} \frac{\partial h}{\partial q} \right)^2 + \left( \frac{UT_w}{h} \frac{\partial h}{\partial T_w} \right)^2 + \left( \frac{UT_b}{h} \frac{\partial h}{\partial T_b} \right)^2 \right]^{1/2}$$

$$\left[ \frac{UNu}{Nu} \right] = \left[ \left( \frac{Uh}{Nu} \frac{\partial Nu}{\partial h} \right)^2 + \left( \frac{Uk}{Nu} \frac{\partial Nu}{\partial k} \right)^2 \right]^{1/2}$$

$$\left[ \frac{URe}{Re} \right] = \left[ \left( \frac{Um}{Re} \frac{\partial Re}{\partial m} \right)^2 + \left( \frac{U\mu}{Re} \frac{\partial Re}{\partial \mu} \right)^2 \right]^{1/2}$$

$$\left[ \frac{Uf}{f} \right] = \left[ \left( \frac{Um}{f} \frac{\partial f}{\partial m} \right)^2 + \left( \frac{U\Delta P}{f} \frac{\partial f}{\partial \Delta P} \right)^2 \right]^{1/2}$$

Table 1 presents the degree of uncertainty for the obtained results, indicating that the empirical findings can be replicated within the reported margins of error.

## 4 Result and discussion

### 4.1 Characterization results of Ag-GO hybrid nanoparticles

Figure 3A presents the X-ray diffraction (XRD) pattern of (GO and Ag-GO hybrid nanoparticles), revealing both broad and sharp peaks. These patterns indicate the formation of Ag over GO, encompassing amorphous and crystalline components. Notably, the appearance of peaks at the diffracted Bragg's angle of  $2\theta = 11.1^\circ$  provides compelling evidence for the presence of graphene oxide (GO) in the GO XRD plot. Conversely, in the Ag-GO plots, intriguing transformations occurred. The disappearance of the diffraction peak at  $11.1^\circ$  and the emergence of an expanded broad peak at  $16.94^\circ(002)$  signify the exfoliation of GO resulting from reduction during the reaction with ascorbic acid in the  $AgNO_3$  solution. Furthermore, this transformation involves the attachment of Ag nanoparticles in the interlayers, effectively masking the GO signals (Hui et al., 2014; Vi et al., 2018). Moreover, distinct peaks observed at  $38.1^\circ$ ,  $44.3^\circ$ ,  $64.5^\circ$ , and  $77.3^\circ$  correspond to the crystallographic plane indices of Ag (111), (200), (220), and (311), respectively, affirming the presence of silver nanoparticles in the samples. The results establish the formation of Ag nanoparticles exhibiting a cubic crystal structure with space group Fm-3 m, consistent with JCPDS Card no. 07-0783 (Hui et al., 2014). Notably, the Ag peak intensities in the Ag-GO XRD

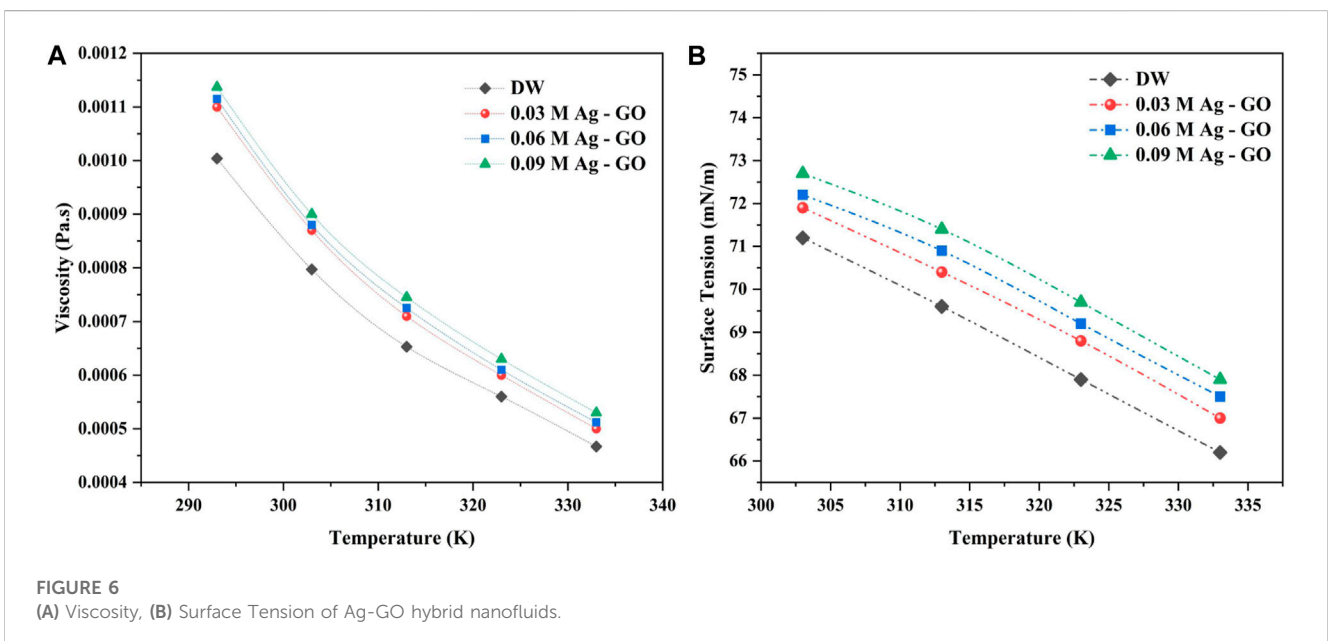
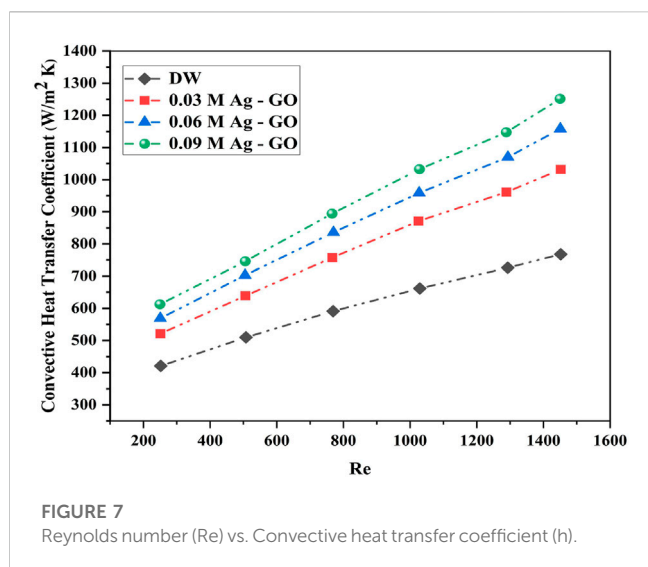


FIGURE 6 (A) Viscosity, (B) Surface Tension of Ag-GO hybrid nanofluids.



plots exhibit a steady increase from 0.03 M to 0.09 M, which indicates varying Ag contents in each sample (Vi et al., 2018).

Figure 3B presents an intriguing comparison of transmittance percentage and wavenumbers between GO and Ag-GO hybrid nanoparticles through FTIR spectrum analysis. Noteworthy spectral bands at  $3,412.08\text{ cm}^{-1}$  and  $1,058.92\text{ cm}^{-1}$  correspond to the O-H bending vibrations of C-OH in carboxylic acid and phenolic acid structural groups, respectively (Cobos et al., 2020). Additionally, the functional bands at  $1,724.6\text{ cm}^{-1}$  and  $1,597.06\text{ cm}^{-1}$  are associated with the asymmetric and symmetric carbonyl stretch vibrations of COOH groups (C=O) (Hui et al., 2014). In the Ag-GO FTIR plot, an intriguing observation emerges— (i) reductions in O-H bending vibrations at both wave numbers ( $3,412.08\text{ cm}^{-1}$  and  $1,058.92\text{ cm}^{-1}$ ), (ii) alongside a reverse change in carbonyl stretching vibrations. The asymmetric ( $1,724.6\text{ cm}^{-1}$ ) stretching decreases, while the symmetric ( $1,597.06\text{ cm}^{-1}$ ) stretching vibration increases. These changes signify the interaction between Ag nanoparticles and the oxygenated functional groups of GO nanosheets, forming a consistent electrostatic attraction or chemical bond (Hui et al., 2014).

In Figure 3C, the Energy Dispersive Spectrum on an SEM revealed the presence of C (K shell), O (K shell), and Ag (M and L shell) in the 0.09 M Ag-GO hybrid sample with weight percentages of 37.8%, 29.3%, and 32.9%, respectively. These results confirmed that the hybrid sample contained both Ag and GO elements.

The UV spectral analysis of Ag-GO nano-hybrids was shown in Figure 3D, which indicated the formation of Ag-GO nano-hybrids. The primary absorption peak of GO nanoparticles was found at 235 nm (GO plot) and 259 nm (Ag-GO plot), corresponding to the  $sp^2$  poly-aromatic (C-C bonds) carbon structures (Cobos et al., 2020). The 402 nm adsorption spectra (Ag-GO) signified the presence of Ag nanoparticles, which were not present in the GO spectrum. The broad peak was mainly due to the second reflection by the Ag nanoparticle ornamented over the surface of the GO nanosheet. Furthermore, the UV-vis absorption of the Ag-GO nano-hybrids showed a shift in the highest peak of GO from 235 to 259 nm, indicating that GO was partially reduced during the

manufacture of Ag-GO nano-hybrids due to the doping of Ag nanoparticles (Hui et al., 2014; Cobos et al., 2020).

Figures 4A, F depicts the TEM and SEM analysis that demonstrated the formation of uniformly embedded quasi-cubical Ag nanoparticles over an amorphous, worm-like silky veil of graphene oxide nanostructures, as previously reported (Mehrali et al., 2016; Cobos et al., 2020). The carboxyl and hydroxyl groups in GO played a crucial role in providing direct binding locations for Ag over GO. The TEM image (Figure 4A) vividly captures the morphological structure and cluster formation of Ag nanoparticles on the GO surface. This captivating visualization is complemented by the lognormal plot analysis in Figure 4C, which reveals a particle size distribution ranging from approximately 3–35 nm for Ag nanoparticles in 0.09 M Ag-GO hybrid nanoparticles, with a standard deviation (SD) of 0.45. Delving deeper into the investigation, a meticulous examination conducted using the High-Resolution Transmission Electron Microscope (HR-TEM) unravels the remarkable face-centered cubic lattice of Ag nanoparticles. This lattice exhibits a precise d-spacing measurement of 0.244 nm, as depicted in the Figures 4D, E. Furthermore, the Selected Area Electron Diffraction (SAED) pattern in Figure 4B during TEM Analysis showcases the  $h\ k\ l$  plane indices, aligning seamlessly with the XRD results. These remarkable findings collectively provide strong evidence, substantiating the success of particle synthesis achieved through a cost-effective chemical reduction method.

## 4.2 Thermophysical properties of hybrid nanofluid

The thermophysical properties of Ag-GO hybrid nanofluids with varying molar concentrations were empirically measured at temperatures ranging from 293 K to 333 K. The results obtained from the thermal conductivity data showed a linear increase in thermal conductivity with increasing temperature and molar concentration of Ag over GO, as depicted in Figure 5.

This enhancement was attributed to various mechanisms such as Brownian motion (D. Li et al., 2020; Lozano-Steinmetz et al., 2022; Nabil et al., 2017), electron-phonon collision (Mateo et al., 2021), lattice vibration due to percolation effect (Yarmand et al., 2015) and enhanced surface area due to the clustering of Ag nanoparticles (Karthikeyan, Philip, and Raj, 2008; Philip and Shima, 2012; Gonçalves et al., 2021) on the GO surface. At 293 K, thermal conductivity enhancement of 8.03%, 11.04%, and 13.71% were observed, while at 333 K, the maximum enhancement of about 17.13%, 22.63%, and 30.12% were achieved at 0.03 M, 0.06 M, and 0.09 M Ag-GO, respectively, compared to the base fluid.

At 293 K, the viscosity of 0.09 M Ag over GO was higher than that of other molar concentrations of nanofluid, but it approached a similar value as the base fluid viscosity, when the temperature increased. Hence, the increase in temperature was found to reduce the viscosity of the hybrid nanofluids. Figure 6A shows that the viscosity of nanofluids increases exponentially with increasing molarity concentration of Ag over GO. Similar to viscosity, as the temperature increased, the surface tension of the hybrid nanofluids steadily reduced (Figure 6B). This

TABLE 2 Comparison of the empirical outcomes with present study.

Nanofluids		Particle concentrations	Operating conditions		Inferences		References
Type	Method of preparation		Flow conditions	Re	Nu	HTC	
Al <sub>2</sub> O <sub>3</sub> -Cu/water	Thermochemical method/ 2 step process	0.1 vol%	Inner pipe/Laminar flow	500–2,500	13.56%	—	Suresh et al. (2012)
Nitrogen doped graphene/aqueous	Hydrothermal process/ 2 step process	0.01,0.02,0.04,0.06 wt%	Inner pipe/Laminar flow, Flow velocity (0.05–0.4 m/s)	290–2,300	—	7%–50%	Mehrali et al. (2016)
GO/DW	Chemical reduction/2 step process	0.01, 0.02 vol%	Inner pipe/Turbulent flow, Flow rate (0.9,1.2,1.5,1.8 L/min)	—	—	48%	Karabulut et al. (2020)
rGO-CuO/DW	Chemical reduction method/2 step process	0.05 w/v %	Inner pipe/Laminar flow, Flow rate (0.5–1 L/min)	800–1,600	23.84%	53.3%	Kumar et al. (2021)
Ag-GO/DW	Chemical reduction method/2 step process	0.05 wt%	Annulus/Laminar flow, Flow rate (8–47 g/s)	250–1,450	33.5%	62.9%	Present study

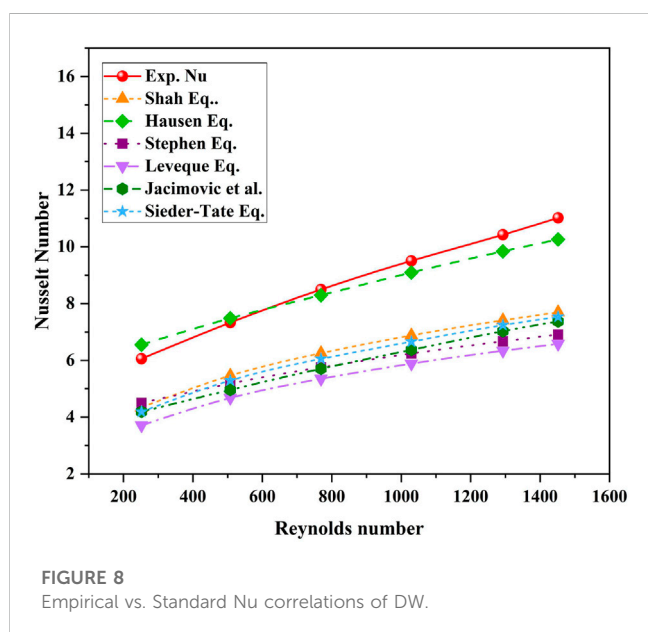


FIGURE 8 Empirical vs. Standard Nu correlations of DW.

reduction was attributed to the increase in Vander Waals force, which increases the surface free energy of the fluid and contributes to better thermal performance (Zheng, 2014; Kamatchi, Venkatachalapathy, and Abhinaya Srinivas, 2015).

## 5 Heat transfer studies

In this study, the empirical investigations have been conducted to elucidate the thermodynamic characteristics and behaviour of varied molarity Ag ornamented GO hybrid nanofluids under laminar flow conditions in a DPHX. Prior to testing the hybrid nanofluids, DW was utilized as the working fluid to establish the dependability and precision of the empirical equipment. Subsequently, the same testing protocol was employed to investigate the hybrid nanofluids and establish a comparison with the base fluid.

### 5.1 Influence of convective heat transfer coefficient

The experimental convective heat transfer coefficient was determined using Eq. 5, and the results were compared with those obtained using DW. Figure 7 depicts the variation of convective heat transfer coefficient ( $h$ ) with Reynolds number ( $Re$ ) for different molar concentrations of Ag ornamented over GO hybrid nanofluids and DW. The scientific findings reveal a significant increase in ' $h$ ' values with an increase in Reynolds number, mass flow rate, and concentration of Ag over GO hybrid nanofluids. Notably, the 0.09 M concentration of Ag-GO exhibited the highest augmentation in  $h$  value (62.9% enhancement) at  $Re=1,451$  and a mass flow rate of 47 g/s, owing to the presence of a larger number of Ag nanoparticles over the GO nanosheets. These Ag nanoparticles acted as thermal enhancement agents and their superior thermal characteristics, combined with GO's thermal properties, contributed to the overall material characteristics, resulting in improved thermal performance of the base fluid.

On the annulus side, the increment in heat transfer coefficient was found to be higher at low Reynolds number compared to the circular inner pipe (Lu and Wang, 2008). However, at  $Re$  250, the heat transfer coefficient deteriorated in all hybrid nanofluids, which may be attributed to axial thermal conduction and a higher frictional factor. The heat transfer coefficient enhancement in other Ag concentrations was found to be 50.82% (0.06 M Ag-GO) and 34.34% (0.03 M Ag-GO) over the base fluid at  $Re$  1,451 and mass flow rate 47 g/s. Since convective heat transfer coefficient is directly proportional to thermal conductivity, the greater impact of thermal conductivity under dynamic conditions also improved the value of  $h$ . The percentage enhancement in  $h$  value indicates the lesser impact of dynamic viscosity of hybrid nanofluids induced by thermophoresis and Brownian diffusion in the tube's midline (Mehrali et al., 2015; Yarmand et al., 2015). Therefore, the thermal performance was improved in the higher molar concentration of Ag over GO compared to other lower concentrations at the same weight percentage of hybrid nanofluids. This study highlights the significance of hybridization in nanoparticles and its flexibility in increasing or decreasing the

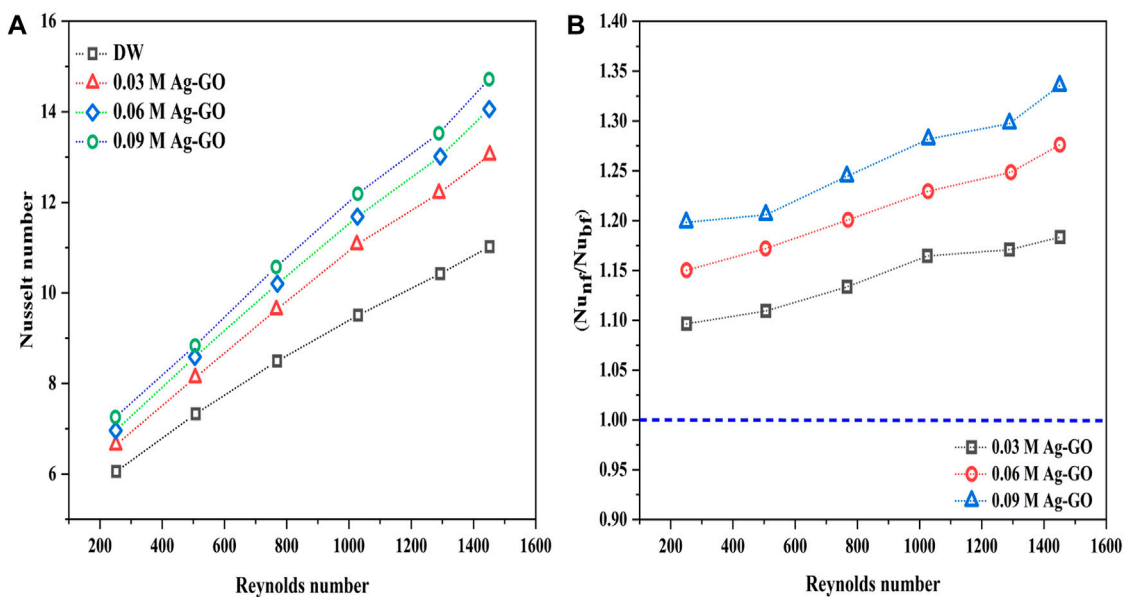


FIGURE 9 (A) Comparison of Nu and (B) Nu ratio with Re of Ag-GO hybrid nanofluids.

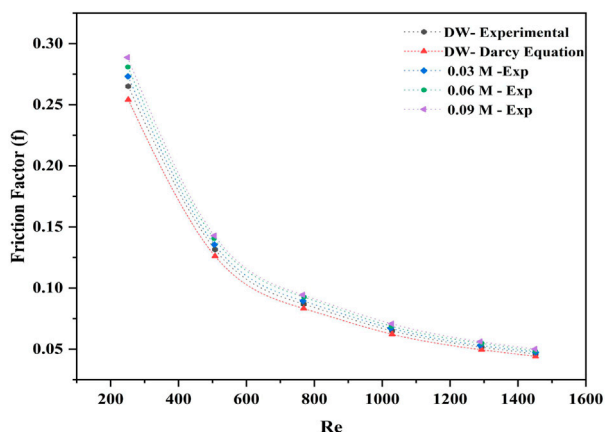


FIGURE 10 Experimental friction factor vs. Theoretical friction factor.

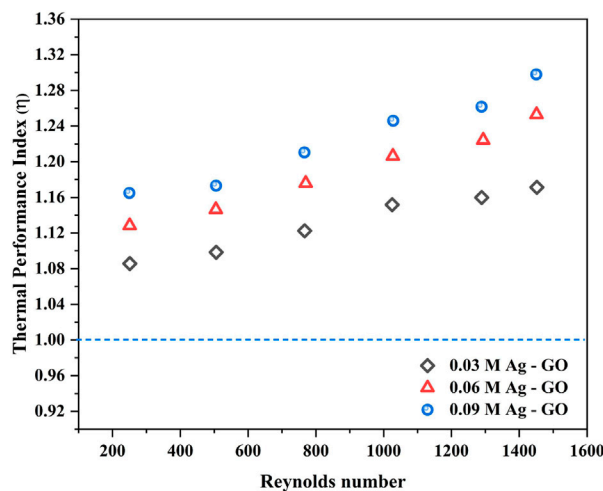


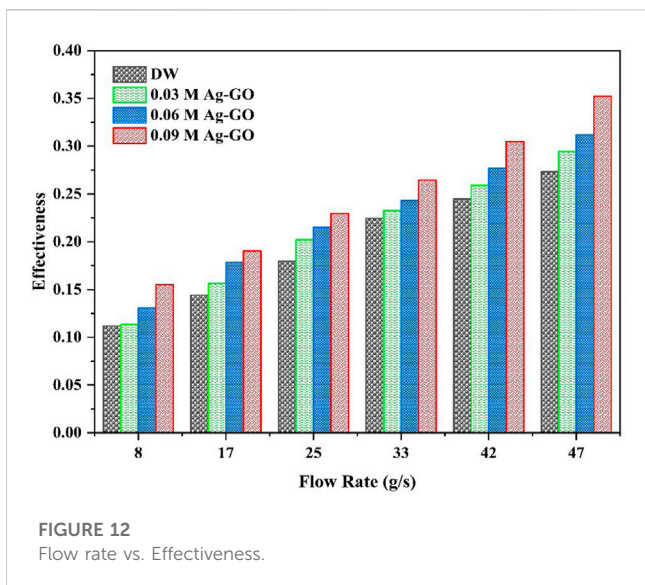
FIGURE 11 Thermal performance index vs. Reynolds number.

molar concentrations of each component, which directly influences the thermal properties of the nanofluids. Table 2 compares the empirical outcomes of the earlier studies to the current study.

### 5.2 Influence of nusselt number

The empirical Nusselt number (Nu) was calculated using Eq. 7, taking into consideration the convective heat transfer coefficient, thermal conductivity, and hydraulic diameter of the annulus pipe. The Reynolds number measured was less than 2,300, indicating laminar flow.

To validate the empirical Nusselt number, standard models of the Nusselt number were used for comparison, and it was observed that the maximum discrepancy between the empirical Nusselt number and the Hausen equation was only around  $\pm 8\%$ , which is well within the acceptable range of  $\pm 10\%$ . Hence, the experimental results were found to be in close agreement with the Hausen correlation (Figure 8). Figure 9A represents the variation of the Nusselt number of DW and hybrid nanofluids with three different concentrations of Ag over GO nanofluids with respect to Reynolds number. The results showed a substantial enhancement in the



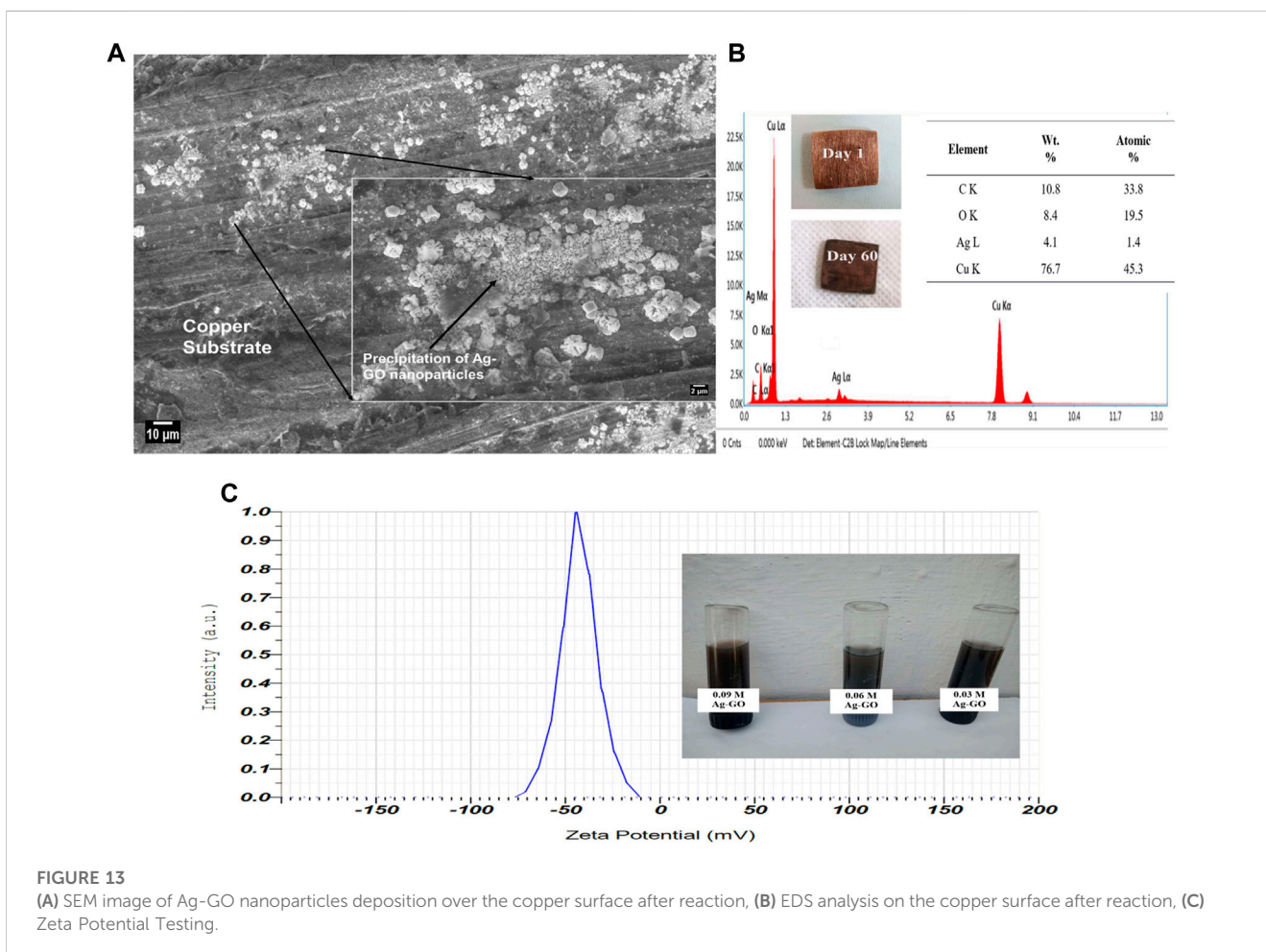
Nusselt number of hybrid nanofluids compared to the base fluid with an increase in Reynolds number, indicating a significant dependency of the Nusselt number on the molar concentration of hybrid nanofluids and Reynolds number. When the Reynolds

number reached 1,451, the Nusselt number exhibited remarkable improvements of 33.55%, 27.62%, and 18.35% using 0.09 M, 0.06 M, and 0.03 M Ag-GO hybrid nanofluids, respectively, compared to the base fluid.

Figure 9B illustrates the Nusselt number ratio ( $Nu_{nf}/Nu_{bf}$ ) of hybrid nanofluids, which provides information on the enhancement of Nusselt number with the addition of nanoparticles in the base fluid. The results indicated that an increase in Reynolds number and molar concentration of nanoparticles enhanced the Nusselt number of the nanofluid. The Nu ratio increased from 1.09 to 1.18 for 0.03 M, from 1.15 to 1.27 for 0.06 M, and from 1.19 to 1.33 for 0.09 M Ag concentration in the Reynolds number ranging from 250 to 1,451 compared to DW.

### 5.3 Influence of friction factor

In Figure 10, the relationship between the observed friction factors and the theoretical friction factor of DW with Reynolds number is depicted. The theoretical friction factor was derived through the Darcy friction factor equation, while the empirical friction factor was estimated by determining the pressure drop on the annulus side. The deviation between these factors demonstrated an excellent agreement with an average deviation of  $\pm 4.1\%$  over Reynolds number.



The results indicated that the experimental friction factors of DW, hybrid nanofluids, and theoretical friction factors decreased closely along the curve line as the Reynolds number increased. At a minimal mass flow rate of 8 g/s and a Reynolds number of 250, the maximum friction factor was observed in 0.09 M, 0.06 M, and 0.03 M Ag-GO of 8.9%, 5.7%, and 3.1%, respectively. This implies that the maximum loss could be found within this range and that it would have lower thermal enhancement than other flow rates and Reynolds numbers. These results demonstrate that dispersing minimal nanoparticles could enhance the pressure drop, which in turn raises the friction factor value at low Reynolds numbers and mass flow rates.

## 5.4 Thermal performance index ( $\eta$ )

Numerous studies have reported that enhancing the heat transfer rate and convective heat transfer coefficient can significantly improve the overall heat-exchanging process. However, accurately predicting the performance of thermal equipment with losses incorporated during experimentation, such as frictional losses, is of utmost importance. The thermal performance index ( $\eta$ ) is a critical factor that can aid in predicting the system's thermal efficiency (Subramanian et al., 2020). Thermal Performance Index is defined as the ratio of the enhancement in the Nusselt number to the enhancement in the friction factor and provides a measure of the system's practical applicability.

Thermal Performance Index (TPI),

$$\eta = \left\{ \frac{(Nu_{nf}/Nu_{bf})}{(f_{nf}/f_{bf})^{1/3}} \right\}$$

A Thermal Performance Index value greater than one is considered indicative of a superior heat transfer system with minimum latency. The molar concentration of Ag relative to GO had a significant impact on the nanofluid's heat transfer ability and performance, especially at higher Re and flow rates. This effect is clearly depicted in Figure 11, which showcases the enhancement of ' $\eta$ ' for all nanofluid configurations. Notably, the nanofluid with 0.09 M Ag concentration over GO yielded the highest thermal performance index value of 1.29 at Re 1,451, indicating that this particular configuration outperformed other Ag concentrations. At the same Re, the other nanofluids exhibited ' $\eta$ ' increments of 1.25 (0.06 M Ag-GO) and 1.17 (0.03 M Ag-GO), demonstrating that even a lower dispersion of Ag over GO can significantly enhance the heat exchanger's performance compared to the base fluid.

## 5.5 Influence of flow rate vs. effectiveness

The effectiveness of the DPHX can be determined by the ratio of the actual heat transfer achieved by the system to the maximum feasible heat transfer, as outlined in Eq. 11. As depicted in Figure 12, the nanofluids demonstrated a more substantial increase in effectiveness across all concentrations of Ag compared to the base fluid. However, both the base fluid and nanofluid showed an increase in effectiveness as the system's mass flow rate increased.

Remarkably, the maximum efficacy was achieved at a flow rate of 47 g/s and with 0.09 M, 0.06 M, and 0.03 M concentrations of Ag over GO hybrid nanofluid, resulting in efficacy values of 35.2%, 31.1%, and 29.4%, respectively.

## 6 Reactivity and stability analysis of Ag-GO hybrid nanofluids

The reactivity of the hybrid nanoparticles over the copper surface was investigated using SEM and EDS, as shown in Figures 13A, B. A sample of the copper substrate from DPHX was collected and immersed in a 0.06 M Ag-GO hybrid nanofluid for 60 days in a closed glass vessel. The SEM and EDS data demonstrated that due to the oxidation and reduction process with the copper substrate, a specific percentage of Ag-GO nanoparticles were deposited over the copper substrate, as the silver particles are highly reactive with copper (Armstrong et al., 2021b; Armstrong et al., 2021a). This observation revealed that the Ag-GO coating over the copper substrate also improved the heat transfer rate in the DPHX by enhancing the surface chemistry of the pipe material.

In order to assess the stability of the Ag-GO hybrid nanofluids, it is necessary to measure the surface charge of the nanoparticles at the interface layer between the solid surface and the dispersed liquid medium. This measurement, known as the Zeta potential or electrokinetic potential, plays a critical role in governing the particle's aggregation or flocculation within the fluid. The higher the surface charge, the more stable the nanofluid (Tharayil et al., 2016). As shown in Figure 13C, the mean Zeta potential value of the 0.09 M Ag-GO hybrid nanofluid was  $-43.6$  mV, indicating that the nanoparticles have a large negative surface charge near the edge of the diffuse layer, thereby demonstrating excellent stability. This stability was achieved by maintaining a pH value of 7.4–7.6 during the preparation of all nanofluids. This study helped us to understand the significant stability span of approximately 25 days with no nanoparticle aggregation.

## 7 Conclusion

This study presents a novel approach to improve the heat transfer efficiency of DPHX using Ag ornamented GO hybrid nanofluids. The heat transfer analysis in DPHX showed a remarkable improvement in the convective heat transfer coefficient and Nusselt number with the addition of Ag-GO hybrid nanofluids. The maximum enhancement was observed with the 0.09 M Ag-GO hybrid nanofluid at a flow rate of 47 g/s and Re 1,451. The friction factor was also found to decrease with the rise in mass flow rate and Re, with the maximum increment identified at Re 250 (0.09 M Ag-GO). The overall effectiveness and thermal performance index were observed to be 35.2% and 1.29, respectively, for the 0.09 M Ag-GO hybrid nanofluid at a flow rate of 47 g/s. In conclusion, this study has shown that increasing the Ag concentration in GO significantly enhances the thermophysical characteristics and heat transfer phenomena in DPHX. The 0.09 M Ag-GO hybrid nanofluid exhibited the best performance among all the tested concentrations. Our findings suggest that the material's

molarity plays a critical role in nanoparticle synthesis for comprehensive heat transfer augmentation in any application. This research can pave the way for further studies on change in molarities of nanoparticles and their application in the thermal management of various industrial processes.

## Data availability statement

The original contributions presented in the study are included in the article/Supplementary material, further inquiries can be directed to the corresponding authors.

## Author contributions

MA: conceptualized and designed the study, synthesized and characterized the nanofluids, conducted the experiments, analysed and interpreted the data, curated the results, and wrote the original draft. SM: provided supervision and guidance throughout the study and proofread the manuscript. NS: provided guidance and co-supervision in the synthesis of nanoparticles and preparation of hybrid nanofluids. CS, SP, and CF: provided co-supervision and proofread the manuscript. All authors contributed to the article and approved the submitted version.

## References

- Armstrong, M., Sivasubramanian, M., and Selva Palam, N. (2021a). Experimental investigation on the heat transfer performance analysis in silver nano-coated double pipe heat exchanger using displacement reaction. *Mater. Today Proc.* 45, 2482–2490. doi:10.1016/j.matpr.2020.11.100
- Armstrong, M., Sivasubramanian, M., Selva Palam, N., Adam Khan, M., and Rajaganapathy, C. (2021b). A recent examination on the nano coating techniques in heat transfer applications. *Mater. Today Proc.* 46, 7942–7947. doi:10.1016/j.matpr.2021.02.660
- Banerjee, Arghya Narayan (2018). Graphene and its derivatives as biomedical materials: Future prospects and challenges. *Interface Focus* 8 (3). doi:10.1098/rsfs.2017.0056
- Bertsche, Dirk, Paul, Knipper, Dietrich, Benjamin, and Wetzel, Thomas (2015). The generalized lévêque equation and its application to circular pipe flow. *Int. J. Heat Mass Transf.* 90 (August), 1255–1265. doi:10.1016/j.ijheatmasstransfer.2015.06.083
- Boudraa, Bouziane, and Bessaïh, Rachid (2021). Turbulent forced convection and entropy generation of impinging jets of water-Al<sub>2</sub>O<sub>3</sub> nanofluid on heated blocks. *J. Appl. Comput. Mech.* 7 (4). doi:10.22055/JACM.2020.35216.2599
- Brebbia, C. A., and Rahman, M. (2000). *Advances in fluid mechanics III*. Cambridge, UK: WIT.
- Cheedarala, Ravi Kumar, and JungSong, Il (2019). *In situ* generated hydrophobic micro ripples via  $\pi$ - $\pi$  stacked pop-up reduced graphene oxide nanoflakes for extended critical heat flux and thermal conductivities. *RSC Adv.* 9 (54), 31735–31746. doi:10.1039/c9ra04563e
- Cheedarala, Ravi Kumar, Park, Eun Ju, YoungPark, Bin, and Park, Hyung Wook (2015). Highly wettable CuO:graphene oxide core-shell porous nanocomposites for enhanced critical heat flux. *Phys. Status Solidi (A) Appl. Mater. Sci.* 212 (8), 1756–1766. doi:10.1002/pssa.201413185
- Cheedarala, Ravi Kumar, Park, Eunju, Kong, Kyungil, YoungPark, Bin, and Park, Hyung Wook (2016). Experimental study on critical heat flux of highly efficient soft hydrophilic CuO-chitosan nanofluid templates. *Int. J. Heat Mass Transf.* 100, 396–406. doi:10.1016/j.ijheatmasstransfer.2016.04.096
- Cobos, Mónica, De-La-pinta, Iker, Quindós, Guillermo, Dolores Fernández, M., and Jesús Fernández, M. (2020). Graphene oxide-silver nanoparticle nanohybrids: Synthesis, characterization, and antimicrobial properties. *Nanomaterials* 10 (2), 376. doi:10.3390/nano10020376
- Duangthongsuk, Weerapun, and Wongwises, Somchai (2009). Heat transfer enhancement and pressure drop characteristics of TiO<sub>2</sub>-water nanofluid in a double-tube counter flow heat exchanger. *Int. J. Heat Mass Transf.* 52 (7–8), 2059–2067. doi:10.1016/j.ijheatmasstransfer.2008.10.023
- Ghalambaz, Mohammad, Jin, Haichuan, Bagheri, Amirhossein, Younis, Obai, and Wen, Dongsheng (2022). Convective flow and heat transfer of nano-encapsulated phase change material (nepcm) dispersions along A vertical surface. *Facta Univ. Ser. Mech. Eng.* 20 (3), 519. doi:10.22190/FUME220603034G
- Gonçalves, Inês, Souza, Reinaldo, Coutinho, Gonçalo, Miranda, João, Moita, Ana, Moreira, António, et al. José Eduardo Pereira (2021). Thermal conductivity of nanofluids: A review on prediction models, controversies and challenges. *Appl. Sci. Switz.* 11, 2525. doi:10.3390/app11062525
- Goodarzi, Marjan, Sh Kherbeet, A., Afrand, Masoud, Sadeghinezhad, Emad, Mehrali, Mohammad, Zahedi, Peyman, et al. (2016). Investigation of heat transfer performance and friction factor of a counter-flow double-pipe heat exchanger using nitrogen-doped, graphene-based nanofluids. *Int. Commun. Heat Mass Transf.* 76 (August), 16–23. doi:10.1016/j.icheatmasstransfer.2016.05.018
- Gul, Waheed, Syed Riaz Akbar ShahKhan, Afzal, Ahmad, Naveed, Ahmed, Sheraz, Ain, Noor, Mehmood, Arshad, Bashir Salah Syed Sajid Ullahand Khan, Razaullah (2023). Synthesis of graphene oxide (GO) and reduced graphene oxide (RGO) and their application as nano-fillers to improve the physical and mechanical properties of medium density fiberboard. *Front. Mater.* 10 (June), 1–10. doi:10.3389/fmats.2023.1206918
- Hui, K. S., Hui, K. N., Dinh, D. A., Tsang, C. H., Cho, Y. R., Zhou, Wei, et al. (2014). Green synthesis of dimension-controlled silver nanoparticle-graphene oxide with *in situ* ultrasonication. *Acta Mater.* 64 (February), 326–332. doi:10.1016/j.actamat.2013.10.045
- Hummers, W. S., and Offeman, R. E. (1958). Preparation of graphitic oxide. *J. Am. Chem. Soc.* 80 (March), 1339. doi:10.1021/ja01539a017
- Hussein, Adnan Mohammed (2017). Thermal performance and thermal properties of hybrid nanofluid laminar flow in a double pipe heat exchanger. *Exp. Therm. Fluid Sci.* 88, 37–45. doi:10.1016/j.expthermflusci.2017.05.015
- Iyahraja, S., Selwin Rajadurai, J., Siva Subramanian, B., Siva Subramanian, S., Sivasankar, P., and Subash, S. (2019). Investigation on convective heat transfer and friction factor of silver-water nanofluid under laminar flow – An experimental study. *Heat Mass Transfer/Waerme- Und Stoffuebertragung* 55 (10), 3029–3039. doi:10.1007/s00231-019-02640-y
- Jacimovic, Branislav, Genic, Srbislav, and Lelea, Dorin (2018). Calculation of the heat transfer coefficient for laminar flow in pipes in practical engineering applications. *Heat. Transf. Eng.* 39 (20), 1790–1796. doi:10.1080/01457632.2017.1388949
- Kamatchi, R., Venkatachalapathy, S., and Abhinaya Srinivas, B. (2015). Synthesis, stability, transport properties, and surface wettability of reduced graphene oxide/

## Acknowledgments

The authors would like to extend their sincere appreciation to the management of Kalasalingam Academy of Research and Education, NIT, Trichy, SRM, Chennai and Karunya Institute of Technology and Sciences, Coimbatore which proved to be vital in the development and validation of materials and experiments needed to complete this project.

## Conflict of interest

The authors declare that the research was conducted in the absence of any commercial or financial relationships that could be construed as a potential conflict of interest.

## Publisher's note

All claims expressed in this article are solely those of the authors and do not necessarily represent those of their affiliated organizations, or those of the publisher, the editors and the reviewers. Any product that may be evaluated in this article, or claim that may be made by its manufacturer, is not guaranteed or endorsed by the publisher.

- water nanofluids. *Int. J. Therm. Sci.* 97 (July), 17–25. doi:10.1016/j.ijthermalsci.2015.06.011
- Karabulut, Koray, Buyruk, Ertan, and Kilinc, Ferhat (2020). Experimental and numerical investigation of convection heat transfer in a circular copper tube using graphene oxide nanofluid. *J. Braz. Soc. Mech. Sci. Eng.* 42 (5), 230. doi:10.1007/s40430-020-02319-0
- Karthikeyan, N. R., Philip, John, and Baldev, Raj. (2008). Effect of clustering on the thermal conductivity of nanofluids. *Mater. Chem. Phys.* 109 (1), 50–55. doi:10.1016/j.matchemphys.2007.10.029
- Kern, D. Q. (1950). *Process heat transfer*. New York, NY, USA: Mc Graw Hill.
- Kumar, Krishan, Chauhan, Prathvi Raj, Kumar, Rajan, and Singh Bharj, Rabinder (2022). Irreversibility analysis in Al<sub>2</sub>O<sub>3</sub>-water nanofluid flow with variable property. *Facta Univ. Ser. Mech. Eng.* 20 (3), 503. doi:10.22190/FUME210308050K
- Kumar, Pramanand, Yadav, Babloo, Kumar, Abhishek, Bora, Chandramika, Kumar, Arun, and Das, Subrata (2021). An experimental study on heat transfer performance of GO and RGO-CuO nanofluids in a heat exchanger. *FlatChem* 27 (May), 100245. doi:10.1016/j.flatc.2021.100245
- Le Ba, Thong, Mahian, Omid, Wongwises, Somchai, and Szilágyi, Imre Miklós (2020). Review on the recent progress in the preparation and stability of graphene-based nanofluids. *J. Therm. Analysis Calorim.* 142, 1145–1172. doi:10.1007/s10973-020-09365-9
- Li, Dan, Wang, Yuxiang, Guo, Meng, Song, Mingjun, and Ren, Yang (2020). Preparation and thermophysical properties of graphene oxide-silver hybrid nanofluids. *Bull. Mater. Sci.* 43, 147. doi:10.1007/s12034-020-02146-y
- Li, Haojie, Wang, Yuan, Han, You, Li, Wenpeng, Yang, Lin, Guo, Junheng, et al. (2022). A comprehensive review of heat transfer enhancement and flow characteristics in the concentric pipe heat exchanger. *Powder Technol.* 15. doi:10.1016/j.powtec.2021.117037
- Lozano-SteinmetzMartínez, Felipe, Victor A., Vasco, Diego A., Sepúlveda-Mualin, Alonso, Singh, Dinesh Patrap, and Singh, D. P. (2022). The effect of Ag-decoration on RGO/water nanofluid thermal conductivity and viscosity. *Nanomaterials* 12 (7), 1095. doi:10.3390/nano12071095
- Lu, Guangyao, and Wang, Jing (2008). Experimental investigation on heat transfer characteristics of water flow in a narrow annulus. *Appl. Therm. Eng.* 28 (1), 8–13. doi:10.1016/j.applthermaleng.2007.03.019
- Maghrabie, Hussein M., Khaled, Elsaid, Enas Taha, Sayed, Mohammad Ali, Abdelkareem, Tabbi, Wilberforce, Mohamad, Ramadan, et al. (2021). Intensification of heat exchanger performance utilizing nanofluids. *Int. J. Thermofluids* 10, 100071. doi:10.1016/j.ijft.2021.100071
- Majumder, Pampi, and Gangopadhyay, Rupali (2022). Evolution of graphene oxide (GO)-Based nanohybrid materials with diverse compositions: An overview. *RSC Adv.* 18. doi:10.1039/d1ra06731a
- Mateo, Diego, Luis Cerrillo, Jose, Durini, Sara, and Gascon, Jorge (2021). Fundamentals and applications of photo-thermal catalysis. *Chem. Soc. Rev.* 21. doi:10.1039/d0cs00357c
- Mbambo, M. C., Khamlich, S., Khamliche, T., Moodley, M. K., Kaviyarasu, K., Madiba, I. G., et al. (2020). Remarkable thermal conductivity enhancement in Ag-decorated graphene nanocomposites based nanofluid by laser liquid solid interaction in ethylene glycol. *Sci. Rep.* 10 (1), 10982. doi:10.1038/s41598-020-67418-3
- Mehrali, Mohammad, Sadeghinezhad, Emad, Rosen, Marc A., Latibari, Sara Tahan, and Mehrali, Mehdi Amir Reza Akhiani; Hendrik Simon Cornelis Metselaar (2015). Heat transfer and entropy generation for laminar forced convection flow of graphene nanoplatelets nanofluids in a horizontal tube. *Int. Commun. Heat Mass Transf.* 66 (August), 23–31. doi:10.1016/j.icheatmasstransfer.2015.05.007
- Mehrali, M., Sadeghinezhad, E., Rosen, M. A., Akhiani, A. R., Tahan Latibari, S., Mehrali, M., et al. (2016). Experimental investigation of thermophysical properties, entropy generation and convective heat transfer for a nitrogen-doped graphene nanofluid in a laminar flow regime. *Adv. Powder Technol.* 27 (2), 717–727. doi:10.1016/j.apt.2016.02.028
- Moffat, R. J. (1985). Using uncertainty analysis in the planning of an experiment. *J. Fluids Eng.* 107 (2), 173–178. doi:10.1115/1.3242452
- Mousavi, Seyed Mehdi, Rostami, Mohammadreza Nademi, Yousefi, Mohammad, and Dinarvand, Saeed (2021). Dual solutions for MHD flow of a water-based TiO<sub>2</sub>-Cu hybrid nanofluid over a continuously moving thin needle in presence of thermal radiation. *Rep. Mech. Eng.* 2 (1), 31–40. doi:10.31181/rme200102031m
- Nabil, M. F., Azmi, W. H., Hamid, K. A., Zawawi, N. N. M., Priyandoko, G., and Mamat, R. (2017). Thermo-physical properties of hybrid nanofluids and hybrid nanolubricants: A comprehensive review on performance. *Int. Commun. Heat Mass Transf.* 83 (April), 30–39. doi:10.1016/j.icheatmasstransfer.2017.03.008
- Philip, John, and Shima, P. D. (2012). Thermal properties of nanofluids. *Adv. Colloid Interface Sci.* 81. doi:10.1016/j.cis.2012.08.001
- Ranjbarzadeh, Ramin, Akhgar, Alireza, Taherialekhouhi, Roozbeh, D'Orazio, Annunziata, Mohammad Sajadi, S., Ghaemi, Ferial, et al. (2022). Improve the heat exchanger efficiency via examine the graphene oxide nanoparticles: A comprehensive study of the preparation and stability, predict the thermal conductivity and rheological properties, convection heat transfer and pressure drop. *J. Therm. Analysis Calorim.* 147 (13), 7509–7521. doi:10.1007/s10973-021-11002-y
- Sharma, R. P., and Mishra, S. R. (2022). Metal and metallic oxide nanofluid over a shrinking surface with thermal radiation and heat generation/absorption. *J. Appl. Comput. Mech.* 8 (2). doi:10.22055/jacm.2020.32813.2085
- Subramanian, R., Senthil Kumar, A., Vinayagar, K., and Muthusamy, C. (2020). Experimental analyses on heat transfer performance of TiO<sub>2</sub>-water nanofluid in double-pipe counter-flow heat exchanger for various flow regimes. *J. Therm. Analysis Calorim.* 140 (2), 603–612. doi:10.1007/s10973-019-08887-1
- Suresh, S., Venkataraj, K. P., Selvakumar, P., and Chandrasekar, M. (2012). Effect of Al 2O<sub>3</sub>-Cu/water hybrid nanofluid in heat transfer. *Exp. Therm. Fluid Sci.* 38 (April), 54–60. doi:10.1016/j.expthermflusc.2011.11.007
- Tharayil, Trijo, Asirvatham, Lazarus Godson, Ravindran, Vysakh, and Wongwises, Somchai (2016). Thermal performance of miniature loop heat pipe with graphene-water nanofluid. *Int. J. Heat Mass Transf.* 93 (February), 957–968. doi:10.1016/j.ijheatmasstransfer.2015.11.011
- Thulukkanam, K. (2013). *Heat exchanger design handbook*. 2nd Edition. Boca Raton, FL: CRC Press.
- Vi, Truong Thi Tuong, Rajesh Kumar, Selvaraj, Rout, Bishakh, Liu, Chi Hsien, Chang, Chia Wei, Chen, Chien Hao, et al. Chak Bor Wong; Shingjiang Jessie Lue (2018). The preparation of graphene oxide-silver nanocomposites: The effect of silver loads on gram-positive and gram-negative antibacterial activities. *Nanomaterials* 8 (3), 163. doi:10.3390/nano8030163
- Yarmand, Hooman, Gharekhani, Samira, Ahmadi, Goodarz, Baradaran, Saeid, Montazer, Elham, Sadat Alehashem, Maryam, et al. Seyed Farid Seyed Shirazi; Mohd Nashrul Mohd Zubir (2015). Graphene nanoplatelets-silver hybrid nanofluids for enhanced heat transfer. *Energy Convers. Manag.* 100 (August), 419–428. doi:10.1016/j.enconman.2015.05.023
- Yu, Wang, Li, Sisi, Yang, Haiyan, and Luo, Jie (2020). Progress in the functional modification of graphene/graphene oxide: A review. *RSC Adv.* 71. doi:10.1039/d0ra01068e
- Zheng, Zhao Zhi (2014). Experimental investigation on surface tension of water-based graphene oxide nanofluids. *Adv. Mater. Res.* 1082 (December), 297–301. doi:10.4028/www.scientific.net/amr.1082.297

## Nomenclature

$Q$	Heat transfer rate, W
$\dot{m}$	Mass flow rate, g/s
$Nu$	Nusselt number
$C_{ph}, C_{pc}$	Specific heat capacity, J/kg. k
$T_p, T_o$	Temperatures of the hot fluid entering and leaving the inner pipe, °C
$t_o, t_i$	Temperatures of the cold fluid entering and leaving the annular pipe, °C
$Gz$	Graetz number
$M$	Mass of nanoparticles, g
$\mu$	Viscosity, Ns/m <sup>2</sup>
$Re$	Reynolds number
$A$	Area, m <sup>2</sup>
$C_{min}$	The minimum value of $C_{ph}$ or $C_{pc}$
$Pr$	Prandtl number
$\mu_b/\mu_w$	Coefficient of friction
$h$	Convective heat transfer coefficient, W/m <sup>2</sup> k
$k$	Thermal conductivity, W/m K
$\Delta P$	Change in pressure, N/m <sup>2</sup>
$d_o, D_i$	The inner pipe's outer and outer pipe's internal diameter, m
$\varphi$	Weight percentage, %
$\epsilon$	Effectiveness
$f$	Friction factor
$C_c = \dot{m}_c * C_{pc}$	Heat capacity of cold fluid, J/kg. k
$C_h = \dot{m}_h * C_{ph}$	Heat capacity of hot fluid, J/kg. k
$RT$	Room Temperature
$(\Delta T)_{LMTD}$	Log mean temperature difference
<b>Subscripts</b>	
$avg$	average
$o$	Outer
$i$	inner
$h$	hot
$c$	cold
$b$	bulk
$w$	wall
$nf$	nanofluids